Nano Today 34 (2020) 100910

Contents lists available at ScienceDirect

Nano Today

journal homepage: www.elsevier.com/locate/nanotoday

# Near-infrared heptamethine cyanine dye-based nanoscale coordination polymers with intrinsic nucleus-targeting for low temperature photothermal therapy

Zhenqi Jiang[a,b], Bo Yuan[a], Yinjie Wang[a,b], Zhenni Wei[a], Shan Sun[a], Ozioma Udochukwu Akakuru[a,b], Yong Li[a], Juan Li[a,*], Aiguo Wu[a,*]

[a] Cixi Institute of Biomedical Engineering, CAS Key Laboratory of Magnetic Materials and Devices, Zhejiang Engineering Research Center for Biomedical Materials, Ningbo Institute of Materials Technology and Engineering, Chinese Academy of Sciences, Ningbo, 315201, PR China
[b] University of Chinese Academy of Sciences, Beijing, 100049, PR China

ARTICLE INFO

*Article history:*
Received 25 May 2020
Accepted 7 June 2020

*Keywords:*
Nanoscale coordination polymer
Photothermal therapy
Nucleus targeting
Near-infrared
Heptamethine cyanine

ABSTRACT

Effective photothermal therapy (PTT) under low temperature (< 50 °C) and power density (< 0.4 W/cm$^2$) avoiding the damage of skin and normal organs. Here, we report a novel heptamethine cyanine dye-based nanoscale coordination polymer (NCP), Hf-HI-4COOH, as an exceptionally effective photosensitizer for nucleus-targeting low temperature PTT. Hf-HI-4COOH shows strong near-infrared absorption and high photothermal conversion efficiency (39.51 %). Further, it exhibits intrinsic nucleus-targeting property and cell inhibition under low power density *in vitro*. Moreover, the long blood circulation, high tumor accumulation, and nucleus-targeting contribute to significant inhibition of breast tumors in tumor-bearing mice under low temperature (48 °C) and power density (0.3 W/cm$^2$) without obvious toxicity. In general, we establish a nucleus-targeting Hf-HI-4COOH for enhanced PTT with low temperature and power density.



## Introduction

Photothermal therapy (PTT) under near-infrared (NIR) light is a promising cancer treatment approach [1–4]. It converts light energy to kill cancer cells with high efficiency and selectivity [4,5]. However, the power density of current available photothermal agents is often higher than the human skin-sustainable maximum value (~0.4 W/cm$^2$) permitted by the American National Standards Institute [6]. Furthermore, the required temperature to induce complete cell necrosis is over 50 °C that will not only destroy the tumor but also do harm to nearby normal organs, for the non-specificity of lasers [7]. Therefore, development of strategies to effectively destruct tumor under low power density and temperature would be efficient way to improve tumor therapeutic efficacy [8].

Luckily, nuclei, as the central governor and one of the most thermolabile intracellular structure, was expected to improve PTT efficiency under low power density and temperature [9–12], because the DNA and proteins in nucleus appear to be hypersensitive to heat [13]. Some encouraging attempts to increase PTT efficiency have been explored by increasing accumulation in nuclei [13], including cell-penetrating peptides (CPPs) [14] and amino-rich polymers [15]. Conjugating or assembling CPPs and amino-rich polymers with photosensitizers (PS) could improve nucleus accumulation [6,12,14], but the nucleus-entry capacity of CPPs was limited after conjugation to PS [16]. Additionally, hemagglutination, severe serum inhibition and subsequently rapid clearance from the blood circulation of amino-rich polymers [17] have obstructed the further development of nucleus-targeted PTT. Furthermore, many reported inorganic nanoparticles based-PS are lack of biodegradability and with potential long-term toxicity [18], whilst organic dyes based-PS are easily to be photobleached [19–21], which hinder the progress of these PS in future clinical translation. To settle the above issues, it is important to develop a biocompatible, high photothermal conversion effective PS with strong NIR absorbance, excellent photostability and instinctive nucleus-targeting [22,23].

Nanoscale coordination polymers (NCPs), self-assembling of metal ions and organic ligands, are thought to be a bright nanocarrier platform for tumor imaging and therapy for its intrinsic biodegradability, structural/chemical diversities, and highly enriched functionalities [24–26]. Previous reports reported

* Corresponding authors.
*E-mail addresses:* lij@nimte.ac.cn (J. Li), aiguo@nimte.ac.cn (A. Wu).

https://doi.org/10.1016/j.nantod.2020.100910
1748-0132/

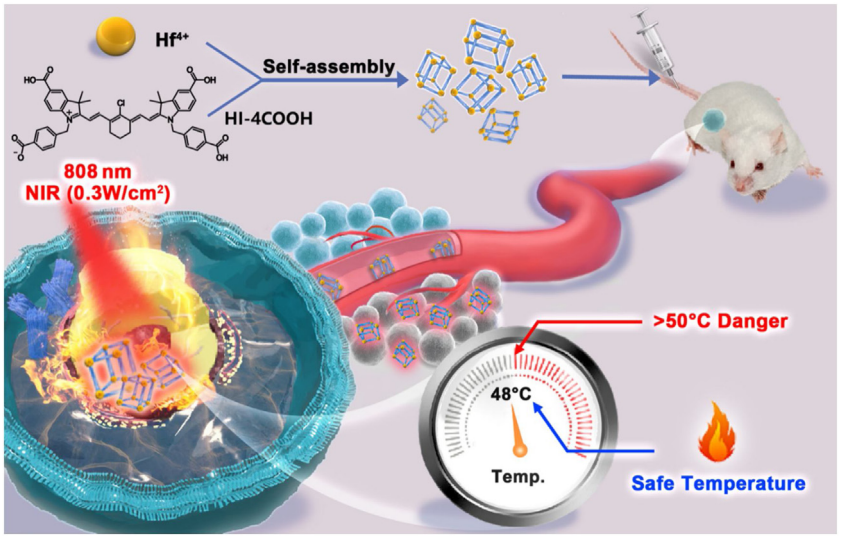


**Scheme 1.** Synthesis of Hf-HI-4COOH NCPs and the description of nucleus targeted low temperature PTT.

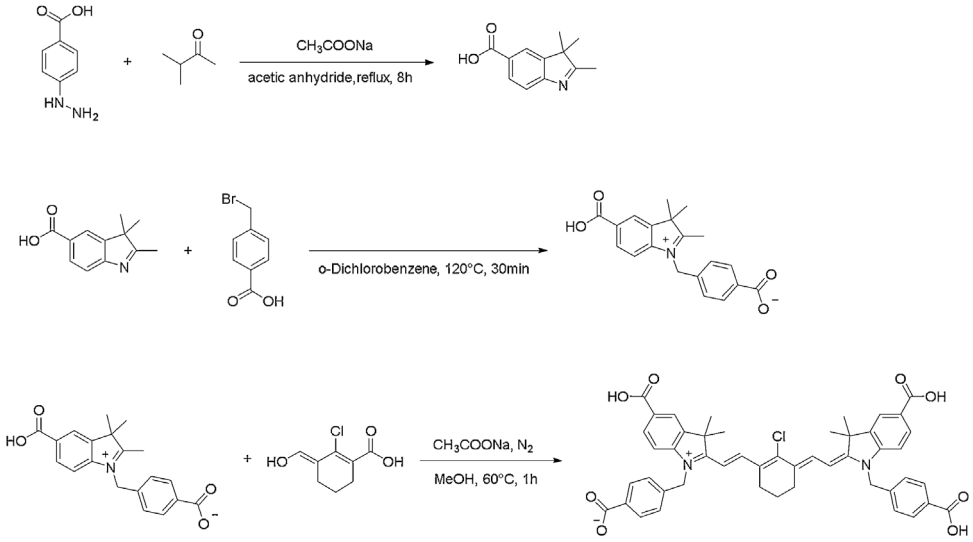


**Scheme 2.** Synthesis path of HI-4COOH.

nanoZIF-90, a subclass of NCPs, improved tumor therapeutic efficacy by mitochondria-targeting without modification [27,28]. Thence, subcellular-targeting NCPs with strong near-infrared absorption and high photothermal conversion efficiency, such as nucleus, might improve therapeutic efficacy of PTT. So far, there were less report about NCPs showed efficient PTT therapy under NIR light, especially with the intrinsic nucleus-targeting ability. We maybe need to develop a new NCPs based on a new designed NIR organic probe.

Herein, we report the synthesis of a Hf-heptamethine indocyanine dye (HI-4COOH)-based NCPs as intrinsic nucleus-targeting PS with highly photothermal conversion efficiency for PTT under low power density and temperature (Scheme 1). For the strong coordination between Hf and carboxyl group and its wide application of Hf in the synthesis of CP [29,30], we choose Hf as a metal element to coordinate with HI-4COOH to form NCPs. Although heptamethine indocyanine dye-based NCPs for PTT have been realized [31], the nucleus-targeting PTT by heptamethine indocyanine dye-based NCPs has not been reported until now. We hypothesized that the incorporation of a heptamethine indocyanine dye-derived bridging ligand into robust NCPs structure of appropriate size would show several advantages compared to the existing PTT agents: first, the dye molecules could be well separated in the polymer, avoiding aggregation and self-quenching under NIR light; second, coordination of heptamethine indocyanine dye ligands to heavy Hf centers *via* the carboxylate of heptamethine indocyanine dye could enhance photothermal conversion efficiency; third, the nucleus-targeting could exert thermal therapeutic effects at low power density and temperature. In this Hf-HI-4COOH design, a high loading of HI-4COOH dye and nucleus targeting can be achieved to allow efficient low power density and temperature PTT. To our best known, this is the first NCPs that shows both intrinsic nucleus-targeting and strong NIR absorption without further modification to increase the tumor inhibition under low power density and temperature.

## Results and discussion

### *Synthesis and characterization of Hf-HI-4COOH*

The newly designed heptamethine indocyanine dye derivative, 4-((5-carboxy-2-((*E*)-2-((*E*)-3-(2-((*E*)-5-carboxy-1-(4-carboxyb-

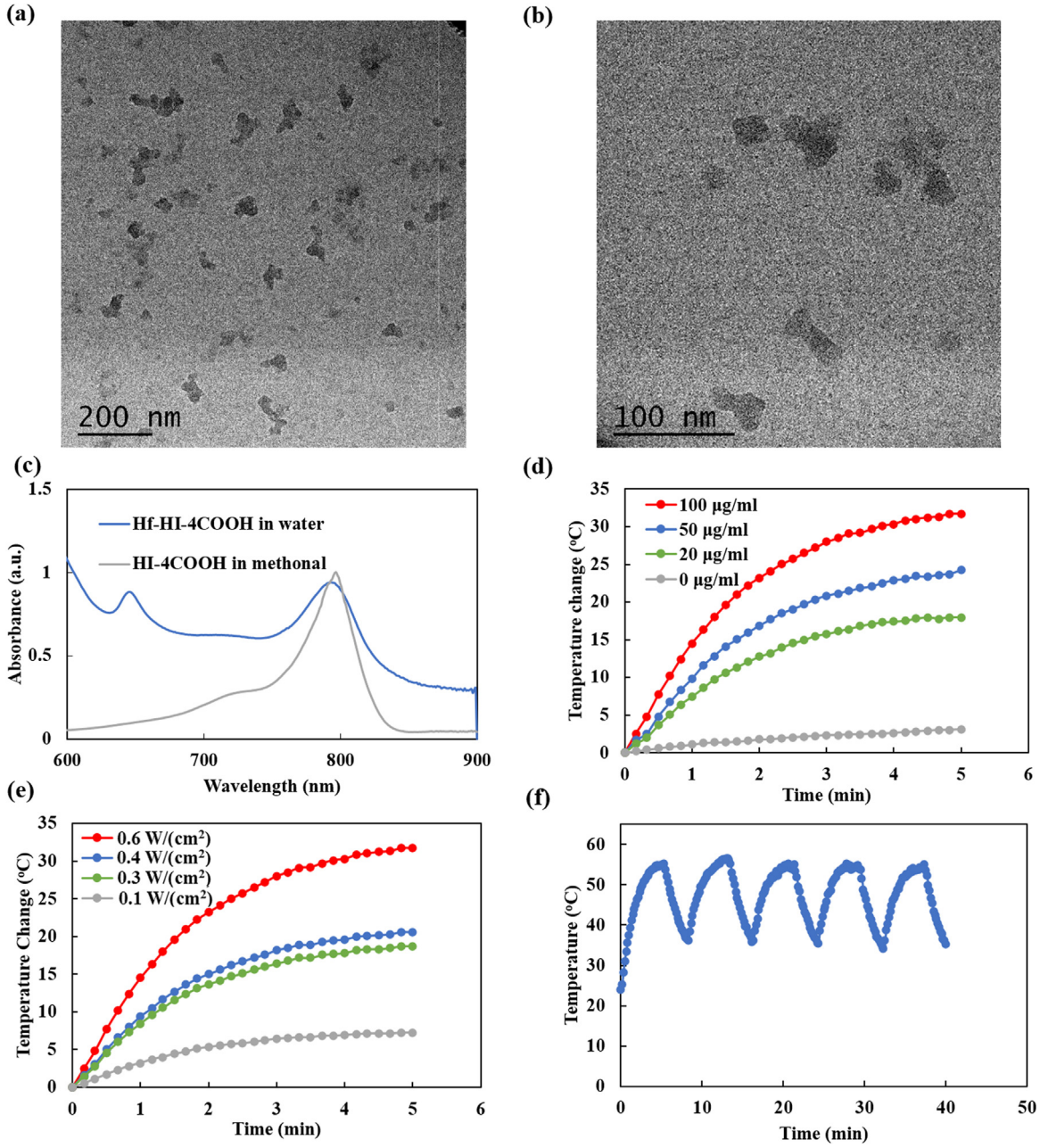


**Fig. 1.** Characterization and photothermal ability of Hf-HI-4COOH. TEM images of (a) Hf-HI-4COOH and (b) incubating in complete RPMI 1640 cell culture medium after 24 h. (c) UV–vis spectra of HI-4COOH in methanol and Hf-HI-4COOH in water. (d) Temperature change of different concentrations of Hf-HI-4COOH solution under an 808 nm laser (0.6 W/cm$^2$). (e) Temperature change of Hf-HI-4COOH (100 μg/mL) solution under different power densities of 808 nm laser. (f) Temperature curves of Hf-HI-4COOH (100 μg/mL) solution for five cycles under an 808 nm laser (0.6 W/cm$^2$).

enzyl)-3,3-dimethylindolin-2-ylidene) ethylidene)-2-chlorocyclohex-1-en-1-yl)vinyl)-3,3-dimethyl-3H-indol-1-ium-1-yl) methyl)benzoate (HI-4COOH), was synthesized by a third-step reaction (Scheme 2), further the structure and chemical components were determined by $^1$H and $^{13}$C NMR and ESI-TOF-MS (Fig. S1-S8). For the strong coordination between Hf and carboxyl groups, the tetra-carboxylate groups of HI-4COOH ligand allow the construction of CPs with Hf. Hf-HI-4COOH NCPs was synthesized through a solvothermal reaction by dissolving $HfCl_4$ and HI-4COOH in N, N-dimethylformamide (DMF) and methanol (MeOH) at 90 °C for 24 h. The resulting product was purified by DMF (two times) and ethanol (four times) successively. By changing the volume of glacial acetic acid (Table S1), we could regulate and control the size of products. The sample 2 showed the highest cellular uptake of Hf (Fig. S11) and was used in subsequent studies.

The obtained Hf-HI-4COOH NCPs showed good dispersibility in water. Powder X-ray diffraction (XRD) measurements and Fast Fourier Transform of the High Resolution TEM image indicated the amorphous nature of Hf-HI-4COOH NCPs (Fig. S12-S13). The TEM image showed the diameter of Hf-HI-4COOH was 30 nm (Fig. 1a). Dynamic light scattering (DLS) measurements showed the average diameter was 36.7 nm for Hf-HI-4COOH (Fig. S14). Notably, this size is smaller than the size that could cross the nucleus pore complex to enter the cell nucleus [32]. Meanwhile, the ζ-potential of Hf-HI-4COOH was −18.4 ± 2.3 mV. The composition of Hf-HI-4COOH was confirmed by plasma optical emission spectrometer (ICP-OES) and organic element analyzer, the ratio of Hf to HI-4COOH was 2.72,

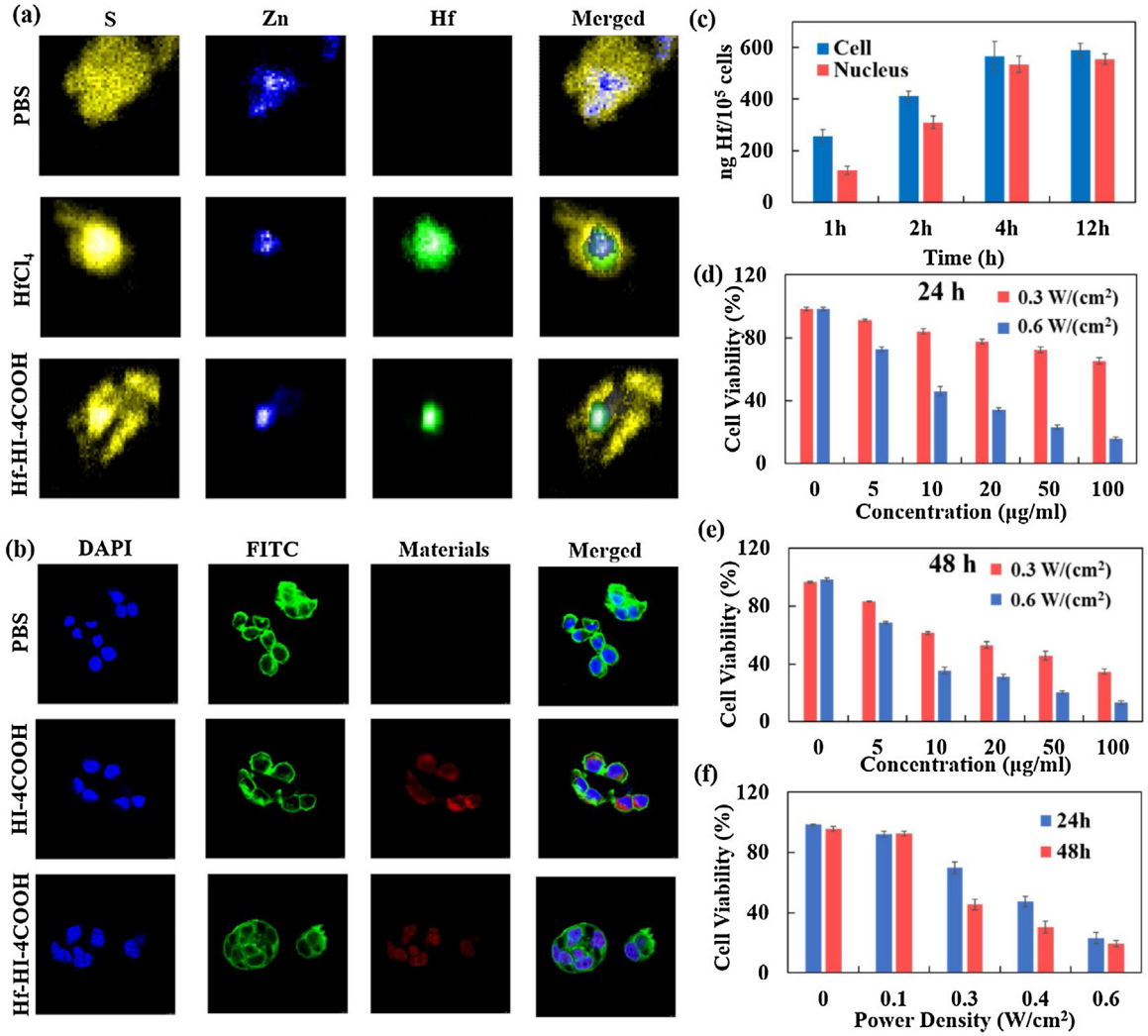


**Fig. 2.** Cellular uptake and PTT efficiency of Hf-HI-4COOH *in vitro*. (a) XFM images of S (cell), Zn (nucleus) and Hf (Hf-HI-4COOH) in 4T1 cells incubated with Hf-HI-4COOH for 8 h. (b) LSCM images of 4T1 cells incubated with Hf-HI-4COOH for 8 h and DAPI was used as a nucleus tracker. (Scale bar = 10 μm) (c) Time-dependent enrichment of Hf-HI-4COOH in the nucleus. (d, e) Cell viability of 4T1 cells incubated with Hf-HI-4COOH for 8 h, then under an 808 nm laser of 0.3 or 0.6 W/cm$^2$ (5 min) and for another 24 and 48 h incubation. (f) Cell viability of 4T1 cells under different power densities of 808 nm laser (5 min) for another 24 and 48 h incubation. The cells were incubated with Hf-HI-4COOH for 8 h before irradiation. Mean ± SD (n = 3).

which was slightly lower than calculated value (the ratio = 3) due to the nano size and defect of Hf-HI-4COOH (Table S2). This result also indicated much carboxylate groups in HI-4COOH were free, which may be the major reason for good water dispersibility and negative ζ-potential of Hf-HI-4COOH. The stability of Hf-HI-4COOH in physiologically relevant media was determined by incubating particles in complete RPMI 1640 medium with 10 % FBS for 24 and 48 h at 37 °C. TEM images and DLS results showed an unaltered morphology and obvious size change after incubation (Fig. 1b, S16a and S17).

*Photothermal ability of Hf-HI-4COOH*

Similar to HI-4COOH in methanol, Hf-HI-4COOH revealed strong absorption at 797 nm (Fig. 1c). The mass extinction coefficient at 808 nm of NCPs was calculated to be 67.11 L/ (g*cm), which was higher than that of many previously reported PSs [18,33]. In addition, the fluorescence of Hf-HI-4COOH was close to the solution under 808 nm laser (Fig. S18), which could improve the effect of PTT [34]. Furthermore, Hf-HI-4COOH showed efficient photothermal conversion efficiency (39.51 %) and could be fastly heated under 808 nm NIR laser (Fig. 1d and e, Table S3). Exposed to NIR laser for five cycles (5 min for one, 0.6 W/cm$^2$), Hf-HI-4COOH showed high photo-stability (Fig. 1f). The TEM images, DLS results and digital photos of Hf-HI-4COOH showed there were no obvious change after NIR laser exposure (Fig. S16b, S17 and S19).

*Cellular location and* in vitro *photo-therapy efficacy of Hf-HI-4COOH*

To confirm the location of Hf-HI-4COOH after incubation with cells, X-ray fluorescence imaging (XFM) and laser scanning confocal microscopy (LSCM) were used [35]. Once cell nucleus was labeled with Zn as previous report [36], the Hf-HI-4COOH were found in nuclei when either Hf or HI-4COOH was used as label while Hf and HI-4COOH were dispersed in the cytoplasm when incubated with only $HfCl_4$ or HI-4COOH (Fig. 2a and b). Furthermore, the Hf contents of cells and nuclei were determined by ICP-OES. The Hf-HI-4COOH could be efficiently internalized into the cells with an uptake percent of about 34 % and 37 % at 4 h and 12 h, respectively. The Hf-HI-4COOH were quickly enriched in nuclei and attained saturation after 4 h incubation. After 4 h, over 90 % of Hf-HI-4COOH internalized by 4T1 cells were found in the nuclei (Fig. 2c). Taken together, Hf-HI-4COOH could be taken up by tumor cells and internalized into their nuclei. To further explore

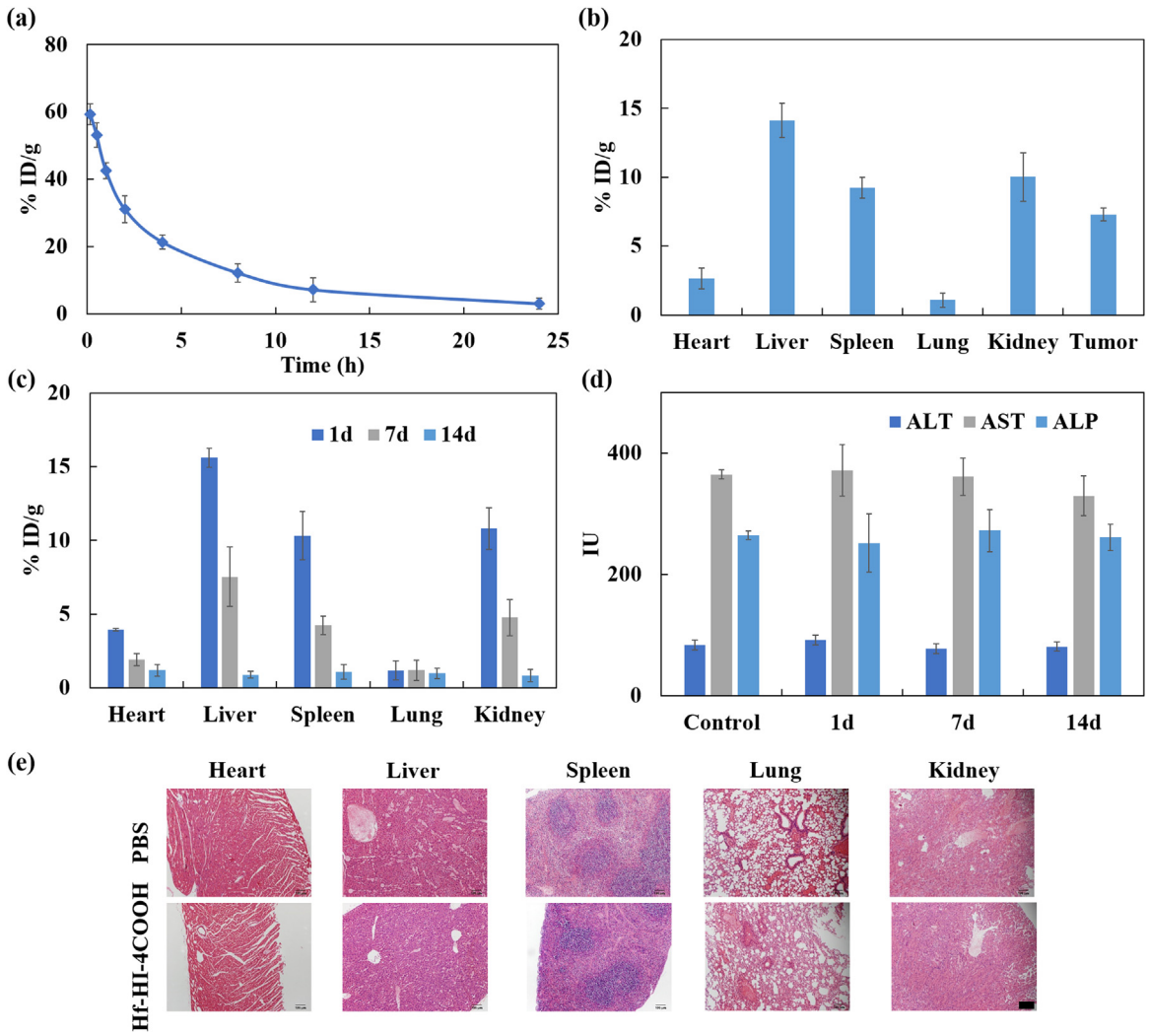


**Fig. 3.** (a) Blood circulation of Hf-HI-4COOH after i.v. injection. The pharmacokinetics followed the two-compartment model. (b) Biodistribution of Hf-HI-4COOH in 4T1-tumor-bearinng mice at 24 h after i.v. injection. (c) Time-dependent distribution of Hf in main organs of healthy mice after i.v. injection of Hf-HI-4COOH. (d) Serum levels of aspartate aminotransferase (AST), alanine aminotransferase (ALT), albumin and alkaline phosphatase (ALP) of health mice after 1, 7 and 14 d post injection (i.v.) of the Hf-HI-4COOH. (e) H&E-stained images of major organs from healthy control mice after i.v. injection of PBS and Hf-HI-4COOH after 60 days (Scale Bar = 100 μm) (The injection dosage of Hf-HI-4COOH was 20 mg/kg).

the mechanism of nucleus-targeting ability, nucleus accumulation of Hf-HI-4COOH with different particle size and zeta potential were investigated (Fig. S11 and S21). These results showed a decrease of nucleus accumulation in 4T1 cancer cells with the particle size increasing, and the zeta potential change from negative to positive with the pH value decreasing. Therefore, proper particle size and positive charge of Hf-HI-4COOH in cancer cells might contribute to the nucleus-targeting. To further compare the nucleus-targeting ability difference of Hf-HI-4COOH between cancer cells and normal cells, the cellular and nucleus accumulation of Hf-HI-4COOH in normal cell line MCF-10A were also tested. Fig. S22 showed the cellular uptake of Hf-HI-4COOH in MCF-10A cells was only one-sixth of 4T1 cancer cells, and less than 30 % of Hf was found in the nucleus of normal cells. Above results showed that both particle size and positive charge contributed to the excellent nucleus-targeting ability of Hf-HI-4COOH in cancer cells [13].

The biocompatibility of the Hf-HI-4COOH was explored by cell counting kit-8 (CCK-8) assay. The results demonstrated that Hf-HI-4COOH showed no obvious toxicity to both cancer and normal cells (ECA-109, 4T1, U87-MG and MCF-10A cells) after being incubated at a high concentration (100 μg/mL) for 24 or 48 h (Fig. S23).

To further evaluate biocompatibility of Hf-HI-4COOH on normal cells, MCF-10A were incubated with Hf-HI-4COOH after different treatment or under NIR laser various concentration. The results showed the Hf-HI-4COOH were biocompatible with normal cells after NIR laser irradiation or high temperature (Fig. S24). In addition, the MCF-10A kept 80 % cell viability after irradiation, indicating normal cells were minimally affected by this treatment (Fig. S25).

To evaluate therapeutic efficacy of Hf-HI-4COOH upon exposure to NIR laser various concentration of Hf-HI-4COOH and laser power were used. The CCK-8 results showed that 4T1 cancer cells can be inhibited within 24 h at a high laser power (0.6 W/cm$^2$) in a concentration-dependent manner for the high temperature. Furthermore, the tumor cells were also inhibited on exposure to a lower laser power (0.3 W/cm$^2$) after 48 h (Fig. 2d, e and f), because cell death caused by heat induced nucleus damage is time-dependent [37]. Afterwards, the apoptosis analysis of 4T1 cells revealed that the major types of induced cell death were different for the 0.3 and 0.6 W/cm$^2$ laser powers, which was early apoptosis and necrosis respectively (Fig. S26).

In vivo *pharmacokinetics and biocompatibility of Hf-HI-4COOH*

Encouraged by the excellent *in vitro* low laser power PTT efficiency, the behavior of Hf-HI-4COOH *in vivo* was also expected. At first, the concentration of $Hf^{4+}$ in blood and major organs were measured by ICP-OES. The concentration of Hf-HI-4COOH in blood showed a gradual decay within 24 h and the half-life was $5.13 \pm 0.35$ h by a two-compartment model (Fig. 3a). The long blood half-life of Hf-HI-4COOH contributed to passive tumor accumulation *via* the enhanced permeability and retention effect. It showed a relatively high tumor accumulation of $7.29 \pm 0.47$ % ID $g^{-1}$ at 24 h post injection of Hf-HI-4COOH for tumor-bearing mice (Fig. 3b). Moreover, the Hf concentration of major organs were tested by ICP-OES. The concentration of Hf decreased to a rather low concentration within 14 days, which indicated that most of Hf-HI-4COOH were cleaned-up from the mice body (Fig. 3c). The side effects of the Hf-HI-4COOH were also important to evaluate safety of Hf-HI-4COOH. The H&E stained major organs of PBS and Hf-HI-4COOH groups also showed that there were no significant signs of inflammatory lesion or organ damage after 60 days (Fig. 3e). Furthermore, blood panel, biochemical and serum analyses were conducted for hematology assay. Within 14 days, the mice treated with Hf-HI-4COOH remained constant compared to the control (Fig. 3d and S27-S29)[38]. All results showed the Hf-HI-4COOH have good biocompatibility and will not result in obvious toxicity during therapy.

*Antitumor efficacy of Hf-HI-4COOH* in vivo

To evaluate the antitumor efficacy *in vivo*, the 4T1 tumor-bearing mice were intravenously administrated with PBS and Hf-HI-4COOH (20 mg/kg). After 24 h the photothermal heating profiles *in vivo* were recorded. There was a rapidly rise ~15 °C within 5 min under 808 nm laser at 0.3 W/$cm^2$ for Hf-HI-4COOH, while the PBS showed only ~1.5 °C increase at the same condition (Fig. 4a and b). Notably, the photothermal heating profile of Hf-HI-4COOH after intratumorally injection were stably within 5 min at 0.6 W/$cm^2$, whilst the HI-4COOH showed an obvious decrease after 2 min (Fig. S30-S33), which indicated that Hf-HI-4COOH showed higher photothermal stability than HI-4COOH *in vivo*. Then the tumors of group which treated by Hf-HI-4COOH with light decreased during the treatment and were eliminated and without recurrence within 14 days post-treatment (Fig. 4c). However, tumors of other three groups showed a rapid growth. Further these mice survived for more than 60 days, whilst the other three groups survived no more than 26 days (Fig. 4d). The body weight of mice after PTT showed no significant decrease, indicating no acute toxicity to mice major organs (Fig. S34). The H&E staining of tumors after treatment also showed that there were much vacuolar chromatin and cell necrosis (Fig. 4e). Comparing to the PBS group, there was no severe damage in other main organs for the mice treated by Hf-HI-4COOH with light, indicating the Hf-HI-4COOH was with good biosafety (Fig. 5 and S35). Besides that, the H&E staining of skins after treatment also showed no obvious damage comparing to the skin of healthy mice (Fig. S36). In general, the Hf-HI-4COOH showed the effective inhibition of tumor growth without obvious toxicity. The nucleus-targeting with high photothermal conversion efficiency of Hf-HI-4COOH contributed to the significantly improved tumor inhibition under low temperature and power density.

## Conclusion

In summary, a newly designed Hf-HI-4COOH for highly effective nucleus-targeted low temperature PTT was developed. The synthesized Hf-HI-4COOH showed great nucleus-targeting and worked as an efficient PS for PTT, as demonstrated by both fast temperature increasement and cytotoxicity assays *in vitro*. PTT efficacy in *in vivo* studies demonstrated tumor decrease under low power density and temperature and complete tumor eradication in mice that were treated with Hf-HI-4COOH without obvious toxicity during the therapy. Further, the Hf-HI-4COOH could be clean-up within 14 days and showed no obvious change of blood analyses. Therefore, the nucleus-targeting Hf-HI-4COOH afford a new generation of highly effective PS for safe PTT under low power density and temperature.

## Experimental section

*Materials and cell lines*

All of the starting materials were purchased from Sigma-Aldrich and Fisher (USA), unless otherwise noted, and used without further purification.

The human esophageal cancer cells ECA-109, mouse breast cancer cells 4T1, human brain glioma cancer cells U87-MG, human epithelial cell line MCF-10A were purchased from Shanghai Cell Bank. The ECA-109 and 4T1 cells were cultured in 1640 medium (Gibco, Grand Island, NY, USA) containing 10 % fetal bovine serum (Hyclone, Utah, USA). U87-MG cells were cultured in MEM medium (Gibco, Grand Island, NY, USA) containing 10 % fetal bovine serum. MCF-10A cells were cultured in Complete culture medium of mammary epithelial cells (Zhongqiaoxinzhou Co.Ltd, Shanghai, China).

*Synthesis of HI-4COOH*

*Synthesis of 2,3,3-trimethyl-3H-indole-5-carboxylic acid*

4-hydrazinobenzoic acid (3.0 g, 19.8 mmol), methyl isopropyl ketone (3.3 mL, 29.7 mmol) and sodium acetate (3.3 g, 39.6 mmol) was mixed in a round-bottomed fitted with a condenser. Another glacial acetic acid (45 mL) was added. The brown suspension was refluxed for 8 h, and the solvent was removed under reduced pressure with a rotavapor. The residue was re-dissolved into a clear solution using 100 mL water and methanol mixture solution (9/1, *v/v*). Undissolved material was filtered off, the filtrate was allowed to stand at room temperature, and the 2,3,3-trimethyl-3H-indole-5-carboxylic acid (2.82 g, 70 %) was collected by filtration. $^1$H-NMR (400 MHz, MeOD, ppm): δ = 8.04 (m, 2 H), 7.51 (t, 1 H), 2.32 (s, 3 H), 1.37 (s, 6 H). *m/z*: calcd., 204.1; found 204.0895. (Fig. S1-S2)

*Synthesis of 5-carboxy-1-(4-carboxybenzyl)-2,3,3-trimethyl-3H-indol-1-ium bromide*

2,3,3-trimethyl-3H-indole-5-carboxylic acid (9.8 g, 48 mmol) and alpha-bromo-p-toluic acid (12.3 g, 57 mmol) were dissolved in 40 mL o-dichlorobenzene and stirring under 120 °C for 30 min. The solid crude product was then filtrated and recrystallized in methanol. The purified product 5-carboxy-1-(4-carboxybenzyl)-2,3,3-trimethyl-3H-indol-1-ium bromide (10.06 g, 62 %) was dried under vacuum. $^1$H-NMR (400 MHz, DMSO-$D_6$, ppm): δ = 8.10 (d, 1 H), 8.00 (d, 3 H), 7.76 (s,2 H), 7.34 (s, 1 H), 3.18 (s, 2 H), 2.40 (s, 3 H), 1.36 (s, 6 H). *m/z*: calcd., 338.1; found 338.1347. (Fig. S3-S4)

*Synthesis of 2-chloro-3-(hydroxymethylidene) cyclohexene-1-carbaldehyde*

80 mL DMF/dichloromethane mixture (1/1, *v/v*) was added dropwisely into a solution of phosphoryl chloride (37 mL) and anhydrous dichloromethane (35 mL) under stirring in ice/water bath; afterwards, 10 g cyclohexanone was added dropwisely. The ice/water bath was removed, and the solution was then heated and refluxed for 3 h. The mixture was poured into ice, yielding a solid

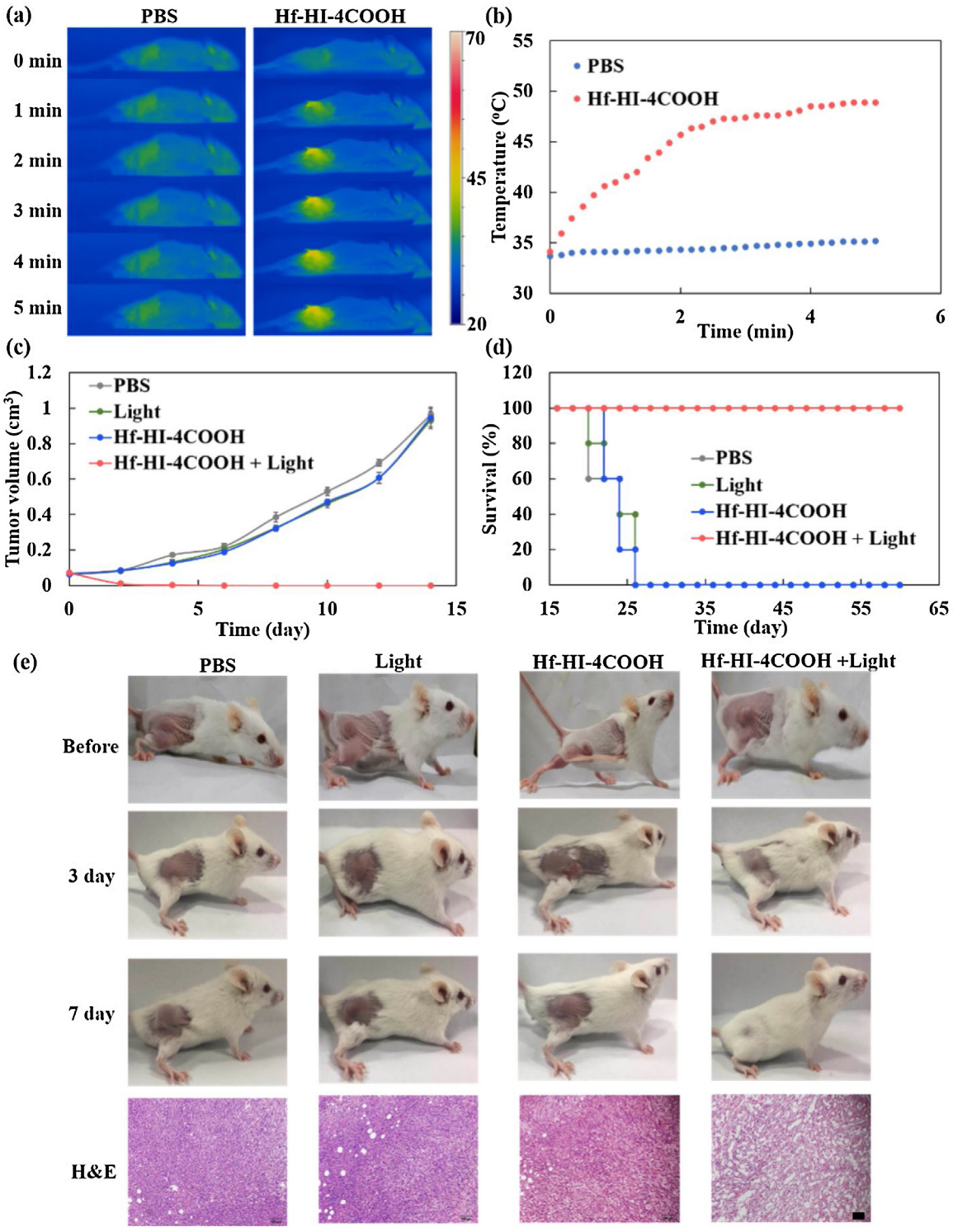


**Fig. 4.** PTT efficiency of Hf-HI-4COOH *in vivo*. (a) IR thermal images and (b) temperature change of 4T1 tumor-bearing mice with intravenous injection PBS or Hf-HI-4COOH under 808 nm (0.3 W/cm$^2$) laser irradiation taken at different time intervals. (c) Tumor volume change and (d) survival rate of tumor-bearing mice after different treatments. Mean ± SD (n = 5). (e) Photography of tumor-bearing mice at 0, 3rd and 7th days treatment and H&E staining of tumors for one treatment after 24 h. (Scale bar = 100 μm).

product which was collected by filtration and washed with iced diethyl ether. The resulting yellow product was used directly.

*Synthesis of HI-4COOH*

5-carboxy-1-(4-carboxybenzyl)-2,3,3-trimethyl-3H-indol-1-ium bromide (1.32 g, 3.9 mmol), 2-chloro-3-(hydroxymethylidene)cyclohexene-1-carbaldehyde (0.34 g, 1.9 mmol) and sodium acetate (1.65 g, 19.8 mmol) were mixed in 260 mL methanol, and stirred for 1 h at 60 °C under $N_2$. The solvent was removed by rotatory evaporation, and the crude product was purified by dissolving in DMF and precipitating in diethyl ether. After filtration, the HI-4COOH (0.984 g, 64 %) was dried under vacuum. $^1$H NMR (400 MHz, MeOD, ppm): δ = 8.43(d, 1 H), 8.34(d, 1 H), 8.25(t, 1 H), 8.18(t, 1 H), 8.13(d,2H), 8.05(d, 2 H), 7.97(d,3 H), 7.31(t, 3 H), 6.28 (s, 1 H), 5.48(s, 3 H), 3.24(s, 2 H), 2.51(s, 2 H), 1.80(t, 12 H), 1.31(m, 6 H). $^{13}$C-NMR (101 MHz, DMSO-$D_6$, ppm): δ = 170.90(a),

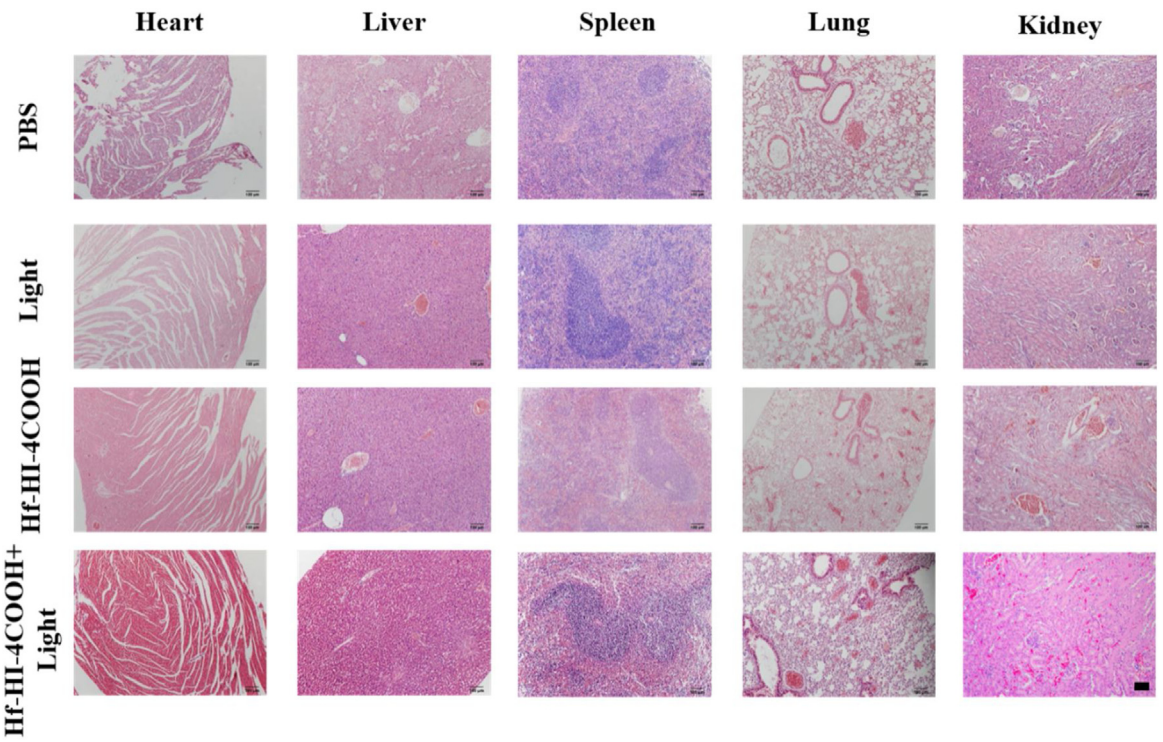


**Fig. 5.** H&E staining of vital organs after tail vein injection of PBS, only light, Hf-HI-4COOH and Hf-HI-4COOH with light for 14 days. (Scale Bar = 100 μm).

168.30(k, ag, ap), 156.31(p), 152.34(aa), 149.79(aj), 148.69(g), 145.77(m), 144.54(ad), 141.65(j), 141.32(af), 138.58(b), 137.94(ao), 132.23(s), 131.05(e), 130.77(al), 130.35(i, l), 130.10(c), 130.00(d), 129.37(w), 128.88(h), 127.17(an), 127.10(am), 126.95(ae, ah), 126.53(aj), 123.32(r), 120.59(y), 106.69(q), 106.36(z), 100.36(q, z), 95.88(x), 60.25(f), 55.54(n), 49.38(ab), 48.67(ak), 28.18(ac), 28.02(o), 21.28(t), 20.46(v), 14.54(u). *m/z*: for $[C_{48}H_{42}ClN_2O_8]$-, calcd. 811.2625; found 811.2276. The purity of HI-4COOH was tested by HPLC (Agilent 1260) (MeOH: water containing 0.1 % $H_3PO_4$ = 75 : 25, flow rate =1 mL/min, temperature: 30 °C, $C_{18}$ column) (97.0562 %). $\varepsilon$(808 m, in MeOH) = $1.342 \times 10^5$ $M^{-1}$ $cm^{-1}$. (Fig. S5-S8)

*Synthesis and characterization of the Hf-HI-4COOH NCPs*

30 mg HI-4COOH and 10 mg $HfCl_4$ was added to a 50 mL reactor. Another 10 mL DMF/MeOH (9/1, *v/v*) and different volume glacial acetic acid (Table S1) was added to get a solution. The reaction mixture was kept in 90 °C for 24 h. The resulting powder was washed with copious amounts of DMF, 1 % triethylamine in ethanol (*v/v*), and ethanol successively. For sample 2 as an example, 11.7 mg product was obtained with a yield of 68.2 % calculated with the concentration of Hf. Sample 2 was used for the rest experiment and named as Hf-HI-4COOH.

Particle size and zeta potential of Hf-HI-4COOH NCPs was measured by a particle size-zeta potential analyzer (Nano-ZS, Malvern, England). High resolution transmission electron microscopy (HRTEM) images were recorded by a Talos (Thermofisher, USA). The structural properties of samples were investigated by X-ray diffraction (XRD) using an X-ray powder diffractometer (XRD, D8 Discover, Bruker AXS). The weight of element was tested by ICP-OES (Optima 2100, Perkin-Elmer, USA) for Hf, organic element analyzer (Elementar, Germany) for N, C and H. In order to determine thermal stability, thermogravimetric and derivative thermogravimetric analysis (TG-DTG) (Pyris Diamond, PerkinElmer, U.S.) were used. TG analysis was performed with an increase in temperature from room temperature to 800 °C, and the heating rate was 10 °C/min. UV absorption of Hf-HI-4COOH NCPs was determined by UV–vis detection (Lambda 950, Perkin Elmer, U.S.).

*Intracellular localization and cellular uptake of NCPs in the cells*

For the investigation of elements uptake in 4T1 cells, X-ray fluorescence microscopy at Shanghai Synchrotron Radiation Facility (SSRF, Shanghai, China) was used as our group pervious reported [28]. In general, the cells were grown on sterile Malay films for 24 h, and then were cultured with Hf-HI-4COOH or $HfCl_4$ (Hf: 5 μg/mL) for another 4 h. After fixing by tissue fixative and washed with pure water, the cells were tested. The hard X-rays BL15U beamline at SSR was also used to get distribution mapping of elements (Cl, Zn and Hf) at the condition of energy of the X-ray was 10 keV with the beam spot was 0.5 × 0.5 μm/(step*s).

For LSCM analysis, confocal culture dishes (NETS Co. U.S) were used for the experiment. 4T1 cells on complete DMEM medium were seeded into each dish at at $1 \times 10^5$ cells and allowed to adhere for 24 h under the condition of 5% $CO_2$ at 37 °C. The medium was then removed and treated with fresh medium containing Hf-HI-4COOH or HI-4COOH solution (HI-4COOH: 10 μg/mL). After further 4 h incubation, the cells were washed three times with PBS to remove any absorbed free nanoparticles. Afterwards, the cells were fixed with 4 % formaldehyde for 30 min, treated with 0.1 % triton for 5 min, and then treated with 1.0 % BSA for 30 min and treated with Phalloidin with Fluorescein Isothiocyanate Labeled (5 μg/mL) and DAPI (10 μg/mL) for 30 min at room temperature.

The 4T1 cells or MCF-10A cells were allowed to adhere for 24 h and then treated by Hf-HI-4COOH (Hf: 5 μg/mL) with for 1, 2, 4, 12 h. After removing the culture medium and washing with PBS for three times, the cells were trypsinized and collected. In order to quantify the nuclear uptake, cell nucleus was separated from cell cytosol by nucleus extraction. The extraction solution consisted 1 mM EDTA, 1 % Triton X-100, 100 mM NaCl, and 10 mM Tris buffer (pH 7.4). The collected cells were treated with the nuclei solution at 4 °C. After 10 min, cell nuclei were collected by centrifugation. The nuclei were treated by aqua regia overnight. The nuclear uptake was tested by

ICP-OES. The cellular uptakes of were detected following the above-mentioned procedure without nuclei extraction.

*Establishment of 4T1 breast tumor xenograft*

Under the approvement of the Regional Ethics Committee for Animal Experiments at Ningbo University (Permit No. SYXK (Zhe) 2019–0005). All Balb/C mice used in this study all bought from Kawensi Biological products sales center (Nanjing, China). To develop the tumor model, 4T1 cells ($1 \times 10^6$) suspended in 100 μl of serum-free 1640 medium were subcutaneously injected into the back of each Balb/c mouse. The tumor size was calculated by the long size for a, the short size for b, $V = a^*b^2/2$. When the tumor grew to 40∼60 $mm^3$, the tumor-bearing mice could be used for further experiment.

*Pharmacokinetics and bio-distribution*

To determine the pharmacokinetics of Hf-HI-4COOH, the mice were intravenously (i.v.) injection with 100 μl Hf-HI-4COOH (HI-4COOH: 20 mg/kg) through the tail vein. The blood was collected from each mouse at indicated time points (0.17, 0.5, 1, 2, 4, 8, 12 and 24 h), weighed and then dissolved with digestive aqua regia to analyze the total amount of Hf in the blood by using ICP-OES.

To evaluate the *in vivo* biodistribution of Hf, three tumor mice were i.v. injection with 100 μl Hf-HI-4COOH (HI-4COOH: 20 mg/kg) through the tail vein. After one day, all the mice were sacrificed, and the major organs and tumors were collected, and then the distribution of Hf was determined by ICP-OES analysis. For ICP-OES analysis, these organs were freeze dried and weighted. All organs were treated in aqua regia for 4 h at 95 °C for dissolution of the tissues.

In vivo *antitumor activity*

To observe the temperature change *in vivo* under 808 nm laser irradiation, when the tumor growth to 60∼80 $mm^3$, the mice were anesthetized and intratumorally (i.t.) injected with HI-4COOH and Hf-HI-4COOH (HI-4COOH: 20 mg/kg) then exposed to an 808 nm laser (0.6 W/$cm^2$) for 5 min. The mice injected with PBS were also exposed to radiation under the same conditions. During laser irradiation, the change in temperature of the tumor site was continuously monitored and imaged using a photothermal imaging system (Ti400, Fluke, USA). One mouse was i.v. injection with Hf-HI-4COOH (HI-4COOH: 20 mg/kg). After 24 h, this mouse was anesthetized then exposed to an 808 nm laser (0.3 W/$cm^2$) for 5 min. The mice injected with PBS were also exposed to radiation under the same conditions. During laser irradiation, the change in temperature of the tumor site was continuously monitored and imaged using a photothermal imaging system.

To evaluate the PTT efficiency, 30 mice were randomly divided into six groups. (1) PBS; (2) PBS + light; (3) Hf-HI-4COOH (i.v.); (4) HI-4COOH (i.t.) + 0.6 W/$cm^2$; (5) Hf-HI-4COOH (i.t.) + 0.6 W/$cm^2$; (6) Hf-HI-4COOH (i.v.) + 0.3 W/$cm^2$. The groups (4) and (5) were exposed to 808 nm laser after i.t. and group (6) were exposed after 24 h. The tumor size and body weight were observed at 2 days interval during the whole process of treatment. After treatment, the survival time and percentage of mice was observed for 60 days and the major organs were stained with Hematoxylin and Eosin (H&E) and examined by an optical microscope (DMI3000, Leica, Germany).

## Author contributions

Z. J., J. L. and A.W conceived the experiments. Z. J., and B.Y. designed and synthesized the HI-4COOH and Hf-HI-4COOH. Z.J., Y.W. and Z.W carried out the experiments and data acquisition. Z.J., S. S. and Y.L. lead in data curation and analysis. Z.J. and J.L. took the lead in writing of original draft and designing the figures. O. U. A. took the lead in revising the manuscript. J.L. and A.W. lead in funding acquisition and project administration. All authors provided critical feedback and worked on the manuscript.

## Declaration of Competing Interest

The authors declare that they have no known competing financial interests or personal relationships that could have appeared to influence the work reported in this paper.

## Acknowledgements

This work was financially supported by National Key R&D Program of China (2018YFC0910601), Natural Science Foundation of China (Grant No. 81871411, 32011530115), Youth Innovation Promotion Association Foundation of CAS (2017340), and Key R&D Program of Zhejiang Province (2020C03110). We would also like to thank Mr. Yong Yang at Ningbo University Hospital for hematological analysis. Furthermore, the authors also thank the use of X-ray fluorescence imaging in Shanghai Synchrotron Radiation Facility at Line BL15U.

## Appendix A. Supplementary data

Supplementary material related to this article can be found, in the online version, at doi:https://doi.org/10.1016/j.nantod.2020.100910.

## References

[1] L. Cheng, C. Wang, L. Feng, K. Yang, Z. Liu, Chem. Rev. 114 (2014) 10869–10939.
[2] H.S. Jung, J.-H. Lee, K. Kim, S. Koo, P. Verwilst, J.L. Sessler, C. Kang, J.S. Kim, J. Am. Chem. Soc. 139 (2017) 9972–9978.
[3] P. Huang, J. Lin, W. Li, P. Rong, Z. Wang, S. Wang, X. Wang, X. Sun, M. Aronova, G. Niu, R.D. Leapman, Z. Nie, X. Chen, Angew. Chem., Int. Ed. 125 (2013) 14208–14214.
[4] J.-W. Kim, E.I. Galanzha, E.V. Shashkov, H.-M. Moon, V.P. Zharov, Nat. Nanotechnol. 4 (2009) 688.
[5] J. Lee, J. Kim, W.J. Kim, Chem. Mater. 28 (2016) 6417–6424.
[6] H. Yuan, A.M. Fales, T. Vo-Dinh, J. Am. Chem. Soc. 134 (2012) 11358–11361.
[7] C.J. Diederich, Int. J. Hyperthermia 21 (2005) 745–753.
[8] Y. Yang, W. Zhu, Z. Dong, Y. Chao, L. Xu, M. Chen, Z. Liu,Adv. Mater. 29 (2017), 1703588.
[9] W.-H. Chen, G.-F. Luo, X.-Z. Zhang,Adv. Mater. 31 (2019), 1802725.
[10] J.L. Roti Roti, H.H. Kampinga, R.S. Malyapa, W.D. Wright, R.P. vanderWaal, M. Xu, Cell Stress Chaperones 3 (1998) 245–255.
[11] K.-H. Chow, R.E. Factor, K.S. Ullman, Nat. Rev. Cancer 12 (2012) 196–209.
[12] L. Pan, J. Liu, J. Shi, ACS Appl. Mater. Interfaces 9 (2017) 15952–15961.
[13] L. Pan, J. Liu, J. Shi, Chem. Soc. Rev. 47 (2018) 6930–6946.
[14] N. Li, Q. Sun, Z. Yu, X. Gao, W. Pan, X. Wan, B. Tang, ACS Nano 12 (2018) 5197–5206.
[15] P. Xu, E.A. Van Kirk, Y. Zhan, W.J. Murdoch, M. Radosz, Y. Shen, Angew. Chem., Int. Ed. 46 (2007) 4999–5002.
[16] K. Melikov, L.V. Chernomordik, Cell. Mol. Life Sci. 62 (2005) 2739–2749.
[17] M. Kanamala, W.R. Wilson, M. Yang, B.D. Palmer, Z. Wu, Biomaterials 85 (2016) 152–167.
[18] T. Liu, C. Wang, X. Gu, H. Gong, L. Cheng, X. Shi, L. Feng, B. Sun, Z. Liu, Adv. Mater. 26 (2014) 3433–3440.
[19] X. Zhen, J. Zhang, J. Huang, C. Xie, Q. Miao, K. Pu, Angew. Chem., Int. Ed. 57 (2018) 7804–7808.
[20] J. Li, J. Huang, Y. Lyu, J. Huang, Y. Jiang, C. Xie, K. Pu, J. Am. Chem. Soc. 141 (2019) 4073–4079.
[21] X. Zhen, C. Xie, Y. Jiang, X. Ai, B. Xing, K. Pu, Nano Lett. 18 (2018) 1498–1505.
[22] W. Chen, J. Liu, Y. Wang, C. Jiang, B. Yu, Z. Sun, L. Lu, Angew. Chem., Int. Ed. 58 (2019) 6290–6294.
[23] S. Sun, L. Zhang, K. Jiang, A. Wu, H. Lin, Chem. Mater. 28 (2016) 8659–8668.
[24] S.Y. Teresa, M. Angelika, C. Patrick, S. Christian,Adv. Mater. 0 (2018), 1707365.
[25] S. Li, K. Wang, Y. Shi, Y. Cui, B. Chen, B. He, W. Dai, H. Zhang, X. Wang, C. Zhong, H. Wu, Q. Yang, Q. Zhang, Adv. Funct. Mater. 26 (2016) 2715–2727.
[26] P. Horcajada, R. Gref, T. Baati, P.K. Allan, G. Maurin, P. Couvreur, G. Férey, R.E. Morris, C. Serre, Chem. Rev. 112 (2012) 1232–1268.

[27] J. Deng, K. Wang, M. Wang, P. Yu, L. Mao, J. Am. Chem. Soc. 139 (2017) 5877–5882.
[28] Z. Jiang, Y. Wang, L. Sun, B. Yuan, Y. Tian, L. Xiang, Y. Li, Y. Li, J. Li, A. Wu, Biomaterials 197 (2019) 41–50.
[29] K. Lu, C. He, W. Lin, J. Am. Chem. Soc. 136 (2014) 16712–16715.
[30] K. Lu, C. He, N. Guo, C. Chan, K. Ni, R.R. Weichselbaum, W. Lin, J. Am. Chem. Soc. 138 (2016) 12502–12510.
[31] Y. Yang, J. Liu, C. Liang, L. Feng, T. Fu, Z. Dong, Y. Chao, Y. Li, G. Lu, M. Chen, Z. Liu, ACS Nano 10 (2016) 2774–2781.
[32] L. Hanson, W. Zhao, H.-Y. Lou, Z.C. Lin, S.W. Lee, P. Chowdary, Y. Cui, B. Cui, Nat. Nanotechnol. 10 (2015) 554.
[33] J.T. Robinson, S.M. Tabakman, Y. Liang, H. Wang, H. Sanchez Casalongue, D. Vinh, H. Dai, J. Am. Chem. Soc. 133 (2011) 6825–6831.
[34] L. Cheng, W. He, H. Gong, C. Wang, Q. Chen, Z. Cheng, Z. Liu, Adv. Funct. Mater. 23 (2013) 5893–5902.
[35] Z. Jiang, Y. Tian, D. Shan, Y. Wang, E. Gerhard, J. Xia, R. Huang, Y. He, A. Li, J. Tang, H. Ruan, Y. Li, J. Li, J. Yang, A. Wu, Biomaterials 170 (2018) 70–81.
[36] E.A. Rozhkova, I. Ulasov, B. Lai, N.M. Dimitrijevic, M.S. Lesniak, T. Rajh, Nano Lett. 9 (2009) 3337–3342.
[37] B. Hildebrandt, P. Wust, O. Ahlers, A. Dieing, G. Sreenivasa, T. Kerner, R. Felix, H. Riess, Crit. Rev. Oncol. Hemat. 43 (2002) 33–56.
[38] J. Liu, Y. Yang, W. Zhu, X. Yi, Z. Dong, X. Xu, M. Chen, K. Yang, G. Lu, L. Jiang, Z. Liu, Biomaterials 97 (2016) 1–9.